9

Characterization of Lubricant on Ophthalmic Lenses

Nobuyuki Tadokoro
HOYA corporation /VC Company
Japan

1. Introduction

When people started wearing eye-glasses from the 13th century until the middle of 20th century, the glass was the only material used for ophthalmic lenses. However, plastic lenses were rapidly developed and began to be widely used when PPG Industries, Inc. developed CR-39® in 1940; CR-39®, i.e., allyl diglycol carbonate (ADC), is a thermosetting resin that can be used as a lens material with a refractive index of 1.5. The features of this material are as follows: (1) it is a lightweight material (its specific gravity is half of that of glass), (2) it has strong impact resistance (i.e., it is shatter proof, which guarantees high safety), (3) it is stainable (i.e., has high fashionability), and (4) it can be used in a variety of frames (i.e., it has high fashionability or high workability). The quest for thinner lenses led to an increase in the refractive index of lenses, and current lenses have a super-high refractive index of 1.74 or 1.76.

The biggest drawback of plastic lenses was that they could be "easily scratched," but they were improved sufficiently for practical use, by using a hard coating (HC), i.e., an overcoat formed on the plastic substrate. Subsequently, anti-reflection (AR) coating films were added to increase the clearness of the lens, to reduce the reflection from the ophthalmic lens as viewed by another person, and even to enhance measures for preventing scratches. In recent years, further value-adds have been made to plastic lenses, with the use of lubricants in the top layers for increasing durability, preventing contamination due to scratches on spectacle lenses, and facilitating "easy removal" of dirt.

Research on lubricants used for the improvement of tribology characteristics has progressed rapidly; it has been supported from the end of the 1980s by the development of surface analysis methods (Kimachi et al., 1987; Mate et al., 1989; Novotny et al., 1989; Newman et al., 1990; Mate et al., 1991; Toney et al., 1991; Novotny et al., 1994; Sakane et al., 1999; Tani, 1999; Tadokoro et al., 2001; Tadokoro et al., 2003) and by the technology for high-density magnetic disc recording used in personal computers. The main lubricant selected was perfluoropolyether (PFPE), because it possesses thermal stability, oxidation stability, low vapor pressure, low surface tension, and good boundary lubricity. It was effective in reducing the frictional wear of the surfaces of the magnetic disc and magnetic head, and thus, hundreds of thousands of stable data read-and-write operations could be conducted. The main parameters that determine lubricant properties are the structure, thickness, and state of the lubricant, and various methods were used to investigate them.

On the other hand, the purpose of using a lubricant for ophthalmic lenses is to improve a scratch resistance, to prevent contamination, and to facilitate "easy removal" of dirt; the tribology characteristics of such a lubricant are similar to those of the lubricant used on magnetic discs, and has possibilities of application. There are two differences between lubricants used for ophthalmic lenses and those used for magnetic discs: (1) the film thickness of the lubricant used for magnetic discs does not need to be reduced, because the recording density achieved by using the lubricant for the magnetic disc increases exponentially when the gap between the magnetic disc surface and magnetic head is reduced as much as possible (to approximately 1 nm), and (2) the lubricant for ophthalmic lenses needs to be solid, but magnetic discs can be solid or liquid if stiction, in which a magnetic head sticks to the surface of a magnetic disc does not occur. However, in the case of ophthalmic lenses, dirt, dust, and fingerprints frequently block the view of the user, and the user cleans the lenses with water or rubs them with a soft cloth or paper; therefore, liquid lubricants can cause adhesion problems and does not last for a long time. In reality, conference presentations and papers are limited to information provided by the authors (Tadokoro et al, 2009; Tadokoro et al, 2010; Tadokoro et al, 2011). This chapter discusses tribology, with a focus on the characterization of lubricants, and presents analysis and evaluation results based on the film thickness, structure, distribution, and abrasion resistance of lubricants reported by the authors.

2. Scratches and dirt

Figure 1 shows optical microscopic pictures of ophthalmic lens returned by a consumer who complained about the quality. The different colors in the picture demonstrate the peeling of the AR coating films along the scratch, and thus, the small scratches become visible. Details on how and when the lenses were used are unknown, but it must be understood that scratches actually occur and this problem must be taken into account; this picture shows the importance of surface reforming based on the use of lubricants. While scratch-free lenses cannot be made only by modifying lubricants, the lubricant is one of the most important factors that affect the formation of scratches. Figure 2 shows the results of an abrasion test conducted by scrubbing a lens 20 times with 20 kg steel wool for different lubricants. The results show that the formation of scratches can be controlled by changing the structure or the distribution state of the lubricant. Finally as an example of the comparison of dirt adhesion, figure 3 shows the adhesion of cedar pollen on the lens. In Japan, hay fever, a seasonal allergy caused by cedar pollen, is very common (30% of the citizens have this
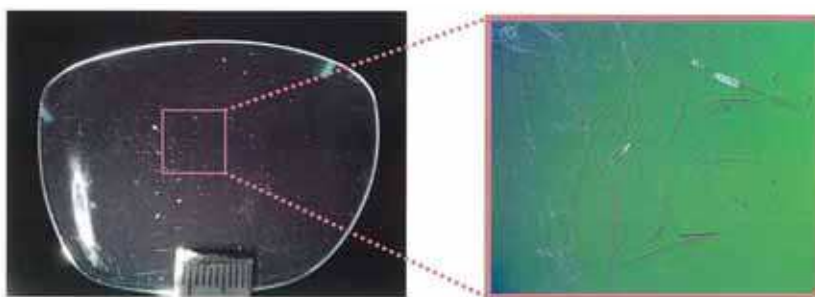

Fig. 1. Damaged ophthalmic lens and scratches

allergy). The results in figure 3 show that changing the surface condition reduces the amount of pollen adhered to the ophthalmic lens brought indoors. As in the example of scratches, the results show the possibility that the surface condition can be controlled to change the amount of dirt that adheres to the lenses.
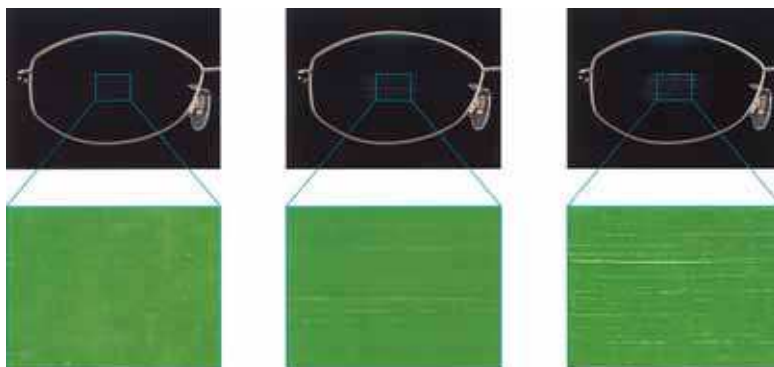

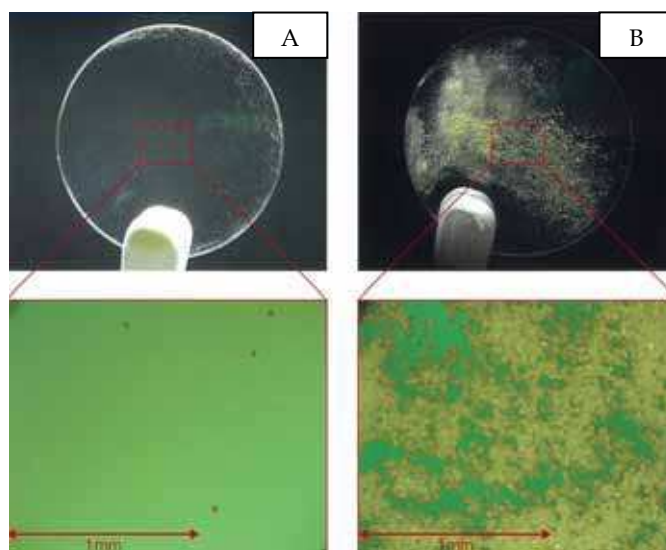Fig. 2. Scratch test results for 3types lubricants: the lens was scrubbed 20 times with 2 kg steel wool

Fig. 3. Comparison between surface condition and cedar pollen adheres to the lens

2.1 Experimental
2.1.1 Sample preparation

Commercial ophthalmic lenses of allyl diglycole carbonate (ADC, CR-39®) were used in this study. In addition, the detailed estimations of lubricants were carried out directly on silicon wafer in order to avoid the influence of surface curvature, roughness, or amorphous states

of actual ophthalmic lenses. The structures of the ophthalmic lenses were as follows: a sol-gel based underlayer on the plastic lens substrate was deposited by dip coating or spin coating methods. The HC material was made using a silica sol and 3-glycidoxypropyltrimethoxysilane. The thickness of HC was approximately 3500 nm. AR coating layers, composed of a sandwich structure between low-index material (SiO_2) and high-index material (Ta_2O_5), were deposited by vacuum deposition methods after the HC underlayer was cleaned by ultrasonic washing with detergent and de-ionized water. The total film thickness was approximately 620nm. The PFPE lubricants, which were also commercial products, were deposited over the AR coating layers by the vacuum deposition methods. The main structure of lubricants A, B, C, G, and H has ($-CF_2-CF_2-O-$)m-(CF_2-O-)n, the main structure of lubricants D and F has ($-CF (CF_3)-CF_2-O-$)m', the main structure of lubricant E has ($-CF_2-CF_2- CF_2-O-$)m''.

2.1.2 Analysis and evaluation methods

The surface morphology and the lubricant film distribution were examined by atomic force microscopy (AFM; Asylum Research, Molecule Force Microscope System MFP-3D). The film thickness, morphology of the cross section, and elemental analysis were used by transmission electron microscopy (TEM-EDS; JEOL, JEM-200FX-2). For the TEM observation, a Cr protective layer was deposited onto the lubricants layer in order to identify a top surface of the lubricants films. The film thickness and the coverage ratio of the lubricant were measured by X-ray photoelectron spectroscopy (XPS; Physical Electronics, PHI ESCA5400MC). Structure analysis was conducted by time-of-flight secondary ion mass spectrometry (TOF-SIMS; ULVAC-PHI, PHI TRIFT-3 or PHI TRIFT-4) and XPS. The wear properties of lubricants were evaluated by contact angle measurement (Kyowa Interface Science Co.,Ltd.; Contact angle meter, model CA-D) and by the use of an abrasion tester (Shinto Scientific Co., Ltd.; Heidon Tribogear, Type 30S). The abrasion test was rubbed in the Dusper K3(Ozu corp.) to have wrapped around the eraser under the condition of 2 kg weight and 600 strokes.

2.2 Results and discussion
2.2.1 Cross-sectional structure, film thickness and coverage of lubricants

Figure 4 shows an example of TEM photograph of lubricant B on a silicon wafer. Figure 5 and figure 6 show an EDS analysis area of TEM photograph and an EDS spectrum of lubricant B. Table 1 summarized the lubricant film thickness and coverage ratio by XPS and TEM. The thickness of the lubricant layer was estimated to be 2.6 nm. And also, we recognized fluorine element in this area by TEM-EDS. These data indicate that both the film thicknesses and the coverage ratios were almost identical across all films. Here, we directly measured the film thickness by TEM. Despite the fact that the lubricant layer was comprised of organic materials, the existence of the lubricant film was directly observed and the film thickness was successfully measured by TEM. Generally, the issue of TEM measurement is sample damage by electron beam. For the reason of successful measurement by TEM, it seems that the lubricant damage of ophthalmic lens is stronger than that of the magnetic disk for electron beam.

It is well-known that the film thickness is proportional to a logarithmic function of the intensity ratio of photoelectrons. According to Seah and Dench (1979), they reported the escape depth of electrons of organic materials with electron kinetic energy by the following

equation; they provide a set of relations for different classes of material over the energy range 1 eV – 6keV (Briggs & Seah, 1990).

$$\lambda_m = 49/E_k^2 + 0.11 \cdot E_k^{0.5} \tag{1}$$

$$\lambda_{lub\ F} = \lambda_m / \rho \tag{2}$$

where $\lambda_{lub\ F}$ is the escape depth of F_{1s} photoelectron of lubricants, λ_m is the escape depth of monolayers for organic materials, E_k is electron kinetic energy, and ρ is the density of material.
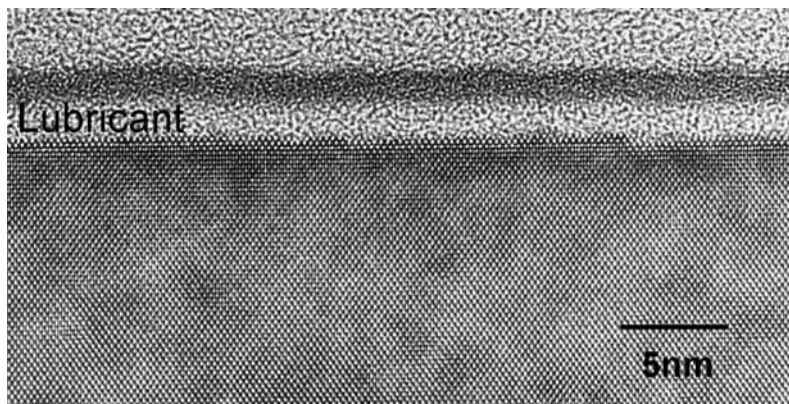

Fig. 4. TEM cross-sectional photograph (glue/Cr layer/lubricant/Si wafer) of lubricant B
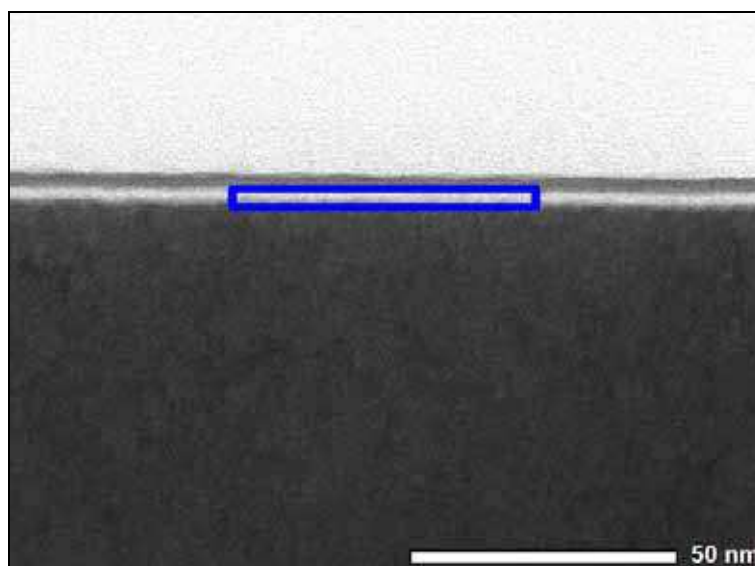
Fig. 5. TEM photograph of lubricant B on a silicon wafer. (Blue area shows the EDS analysis area)
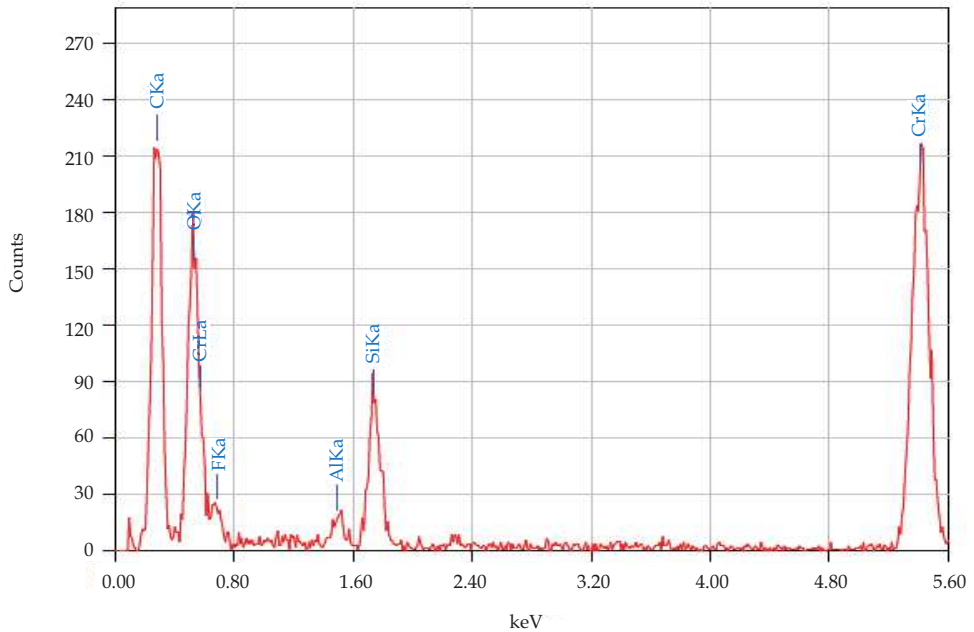
Fig. 6. TEM-EDS spectrum for lubricant B on a silicon wafer

	Lub. film thickness (nm)	Lub. film coverage by XPS (%)	Lub. film coverage by TEM (%)
Sample A	1.5-1.7	98 over	100
Sample B	2.3-2.7	98 over	100
Sample C	2.3-2.7	98 over	100
Sample D	2.1-2.5	98 over	-----
Sample E	1.7-2.2	98 over	-----

Table 1. Film thickness and coverage ratio of lubricant by XPS and TEM

The lubricants film thickness of XPS was calculated by the following equation (3). Table-2 summarizes the parameters used. We experimentally calculated the A factor by using equation (3) from TEM's film thickness and the intensity ration of F_{1s} and Si_{2p} photoelectron (the experimental A factor is 0.116).

$$T = \lambda_{lub\,F} \cdot \sin\theta \cdot \ln\left[\,A \cdot (I_{lub\,F} \,/\, I_{Si}) + 1\,\right] \tag{3}$$

where T is the film thickness of lubricants , θ is the detection angle of XPS measurement, $I_{lub\,F}$ is the intensity of F_{1s} photoelectrons, I_{Si} is the intensity of Si_{2p} photoelectrons, A is the correction factor (calculated value: 0.116, i.e., lubricants films thickness by TEM).

According to Kimachi et al. (1987), they have derived an expression for the coverage ratio of lubricants on magnetic disks using an island model. In the present study, we propose a

modified equation (4) for the coverage of our lubricants using the F_{1s} and the Si_{2p} photoelectrons.

$$A \cdot (I_{lub\,F}/I_{Si}) = \{r \cdot [1-\exp(-T/(\lambda_{lub\,F} \cdot \sin\theta))]\}/\{(1-r)+r \cdot \exp(-T/(\lambda_{Si} \cdot \sin\theta))\} \qquad (4)$$

where r is the coverage ratio from 0 to 1.

Figure 7 shows an example of the relationship between the logarithmic function of the intensity ratio of photoelectron and the coverage ratio. Table 1 already summarized the lubricant film thickness and coverage ratio by XPS and TEM. The coverage ratio of lubricants by XPS is estimated to be over 98%. However, the coverage ratio of TEM seems to be covered a fully 100 % on Si wafer. In case of an actual XPS measurement, a coverage ratio of 100% is unlikely to occur due to the influence of surface roughness, the density of actual lubricants films, and the photoelectron signal of Si_{2p}. Therefore, it seems that the lubricant layer completely covers on the Si wafer when the coverage ratio is approximately 100%. By using this XPS technique, we can easily monitor the lubricant thickness and coverage ratio on a production line for quality control.

	B.E (eV)	$\lambda_{lub\,F}$ (nm)	ρ (kg/m^3)
Lub. F_{1s}	689	1.45	1.8×10^3

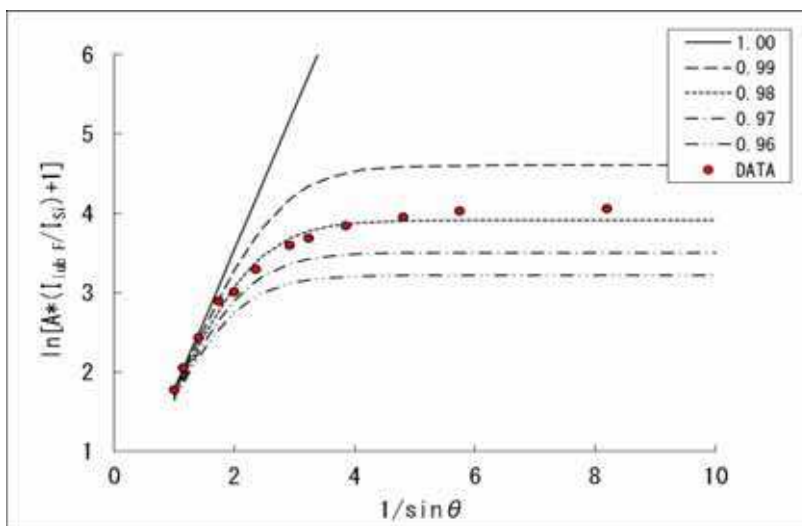Table 2. The escape depth and parameters used

Fig. 7. Coverage calculation results of sample B by XPS measurement

2.2.2 The distribution state of lubricants
Figure 8 illustrates the lubricant distribution of samples A, B, and C by TOF-SIMS analysis. The image was obtained by detecting the positive ion fragments of C+, C2F4+, and Si+. The ion signal intensity is displayed on a scale of relative brightness; bright areas indicate high intensity of each type of fragment ion. Figure 9 shows the comparison of lubricants fragment

ion for samples A, B and C. From fugure-9, we recognized that these samples have same main structure of (-CF$_2$-CF$_2$-O-)m-(CF$_2$-O-)n. The lubricant distribution determined by this analysis was consistent with the actual lubricant distribution. The behavior of the lubricant distribution obtained is attributable to suggest chemical structure and mechanical property of lubricant. Therefore, in terms of elemental fragment ions, the distribution of the lubricant appears to be homogenous at the 10μm scale from figure 8.
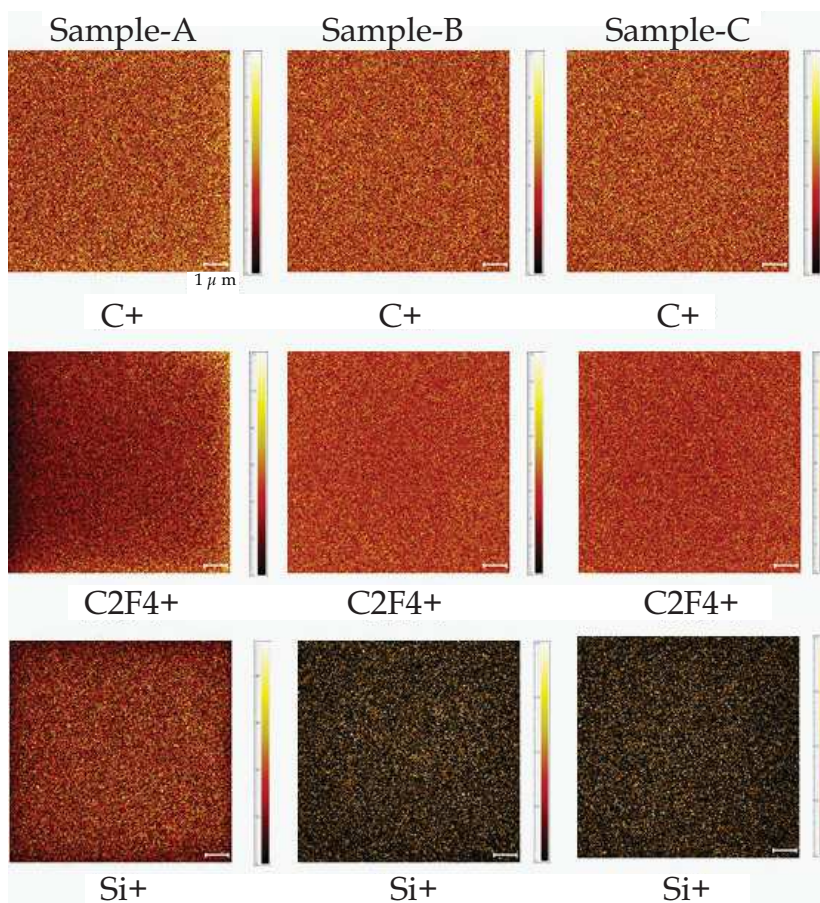
Fig. 8. TOF-SIMS image (C+, C2F4+, and Si+ fragment ions) for each sample

Figure 10 illustrates the lubricant distribution of samples A, B, and C by AFM topographic image and friction force image at the 10 μm scale. Figure 11 shows a frequency analysis of phase separation for sample A and sample B. A red histogram shows the whole area, a blue area shows the phase separation A of lubricants, and a green area shows phase separation B of lubricants. Area distribution of sample 2 has approximately two times larger than that of sample 1. Figure 12 shows the lubricant image of sample B by using phase image and force modulation image. The components between the in-phase (input-i: elasticity) and the quadrature (input-q: viscosity) divided phase image are shown in figure 13. From the TOF-SIMS
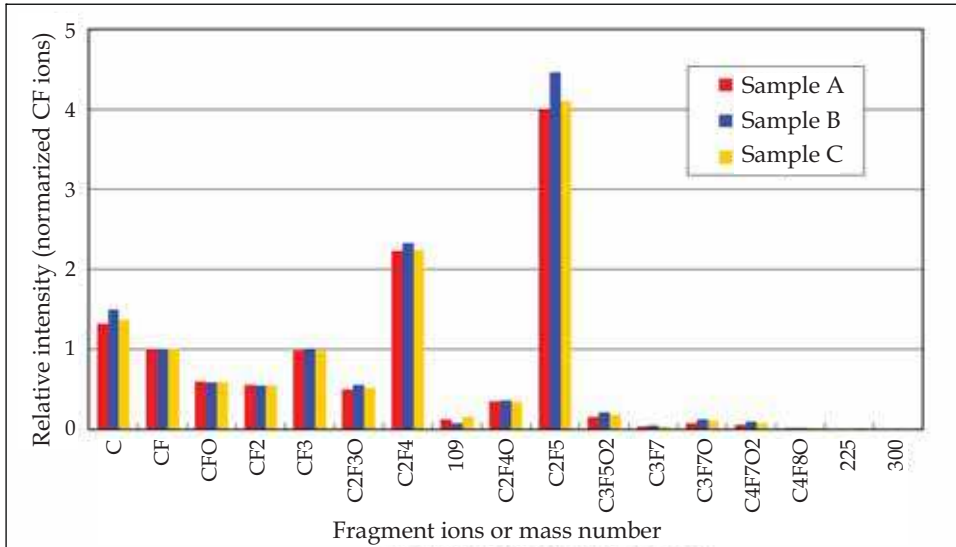
Fig. 9. The comparison of lubricants fragment ion for sample A, B and C

fragment image in figure 8, we recognized the homogeneity of lubricant distribution for sample A, sample B and sample C. However, we found that the uniformity or heterogeneity of an image depended upon the sample and the scale, except for topographic images by AFM measurement added some functionality from figures 10, 12, and 13. Here, in the case of sample B, the friction images agree with the phase images and the phase images agree to the force modulation images. Thus, the friction force image reveals the distribution of friction behavior on the surface. Also, the force modulation image indicates the distribution of hardness; the darker areas correspond to softer areas. Thus, the phase image suggests friction or hardness behavior because it assumes the same image form as the friction force and force modulation.

By friction force microscopy (FFM), the twisting angle is proportional to the tip height of the cantilever in the case of the same cantilever shape and the same material (Matsuyama, 1997).

$$\theta_o = \mu \cdot F_L \cdot (h_t + t/2) \cdot L / (r \cdot G \cdot w \cdot t^3) \tag{5}$$

where θ_o: twisting angle, L: length of cantilever, r: correction factor (calculated value 0.3 to ~0.4), G: shear modulus, w: width of cantilever, t: thickness of cantilever, μ: friction coefficient, F_L: load force, h_t: height of cantilever.

In previous work (Tadokoro et al., 2001), we observed the morphology of lubricants on the magnetic disk surface by FFM. The images of lubricants obtained by a high-response cantilever of tip height 8.4 μm were clearer than those by a standard cantilever of tip height 3 μm in the same load force. The sensitivity of the high-response cantilever was about 2 to 3 times greater than that of the standard cantilever when compared in the same sample area. These observations seemed to experimentally support the theoretical predictions, and the effects of load force for the standard cantilever agree with the theoretical equation. However, FFM has two disadvantages. If the area is too small (i.e., <1 μm) and is low-friction material, the friction force signal is drastically reduced. Moreover, there might be

damage to the lens surface because the friction force image is made by contact. On the other hand, the disadvantage of force modulation methods is that the tip can change shape and is a possible source of contamination because it is always pushed into the sample (indentation). Therefore, we believe that it is more convenient to use phase images than friction force images or force modulation images for determining the island structures of shapes with similar surface morphologies.
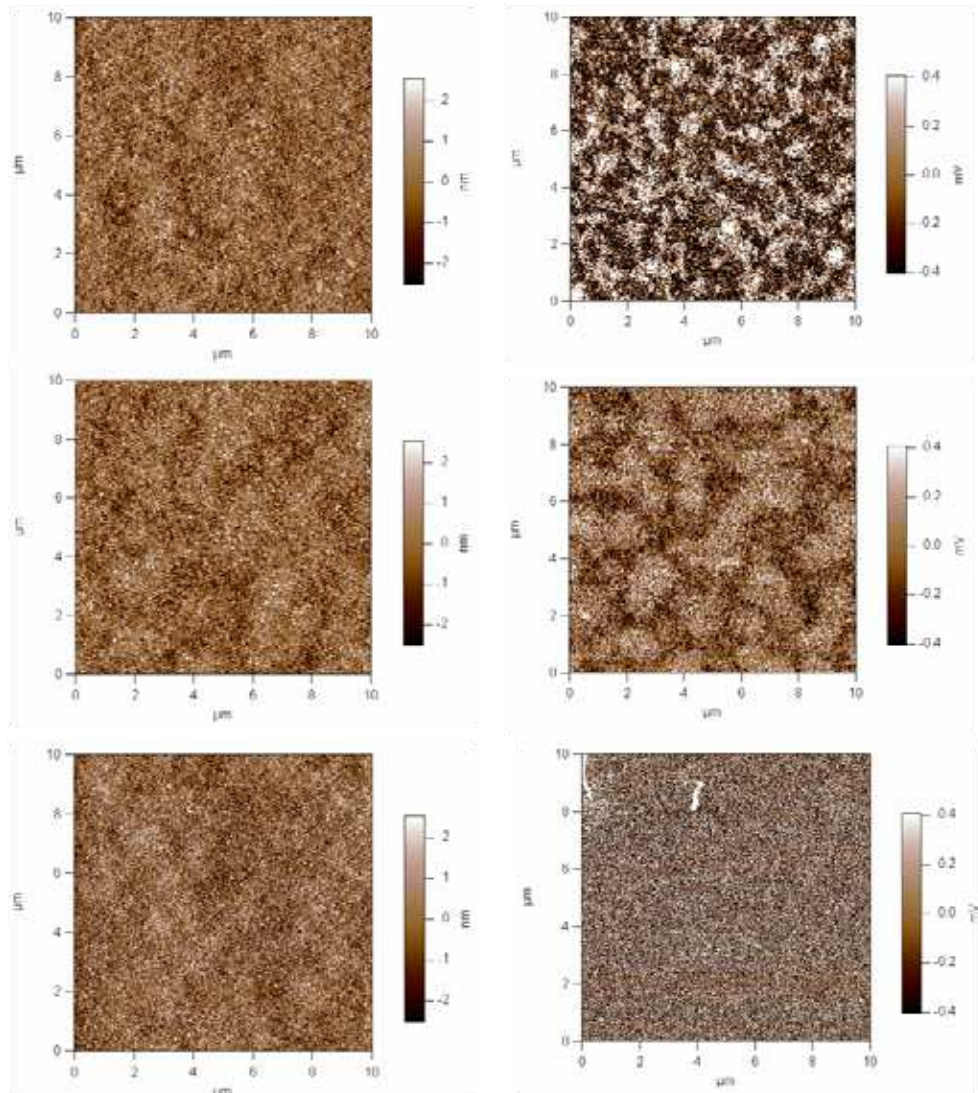

Fig. 10. Topographic image (left side), FFM image (right side; bright area indicates higher friction, darker area indicates lower friction); upper image is sample A, middle image is sample B, lower image is sample C
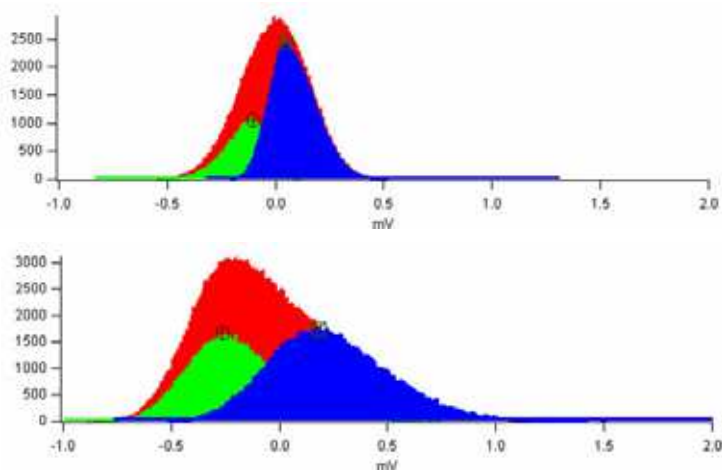
Fig. 11. Frequency analysis of phase separation by FFM (top distribution: sample A, bottom distribution: sample B), it shows red histogram for whole area, blue area for lubricant phase separation A, and green area for lubricant phase separation B
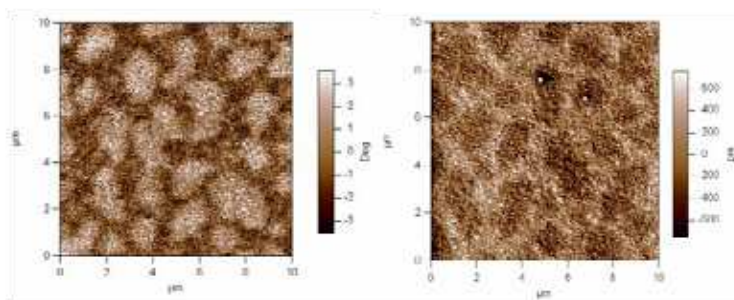
Fig. 12. Phase image (left side), force modulation image (right side; bright area indicates harder area, darker area indicates softer area) of sample B
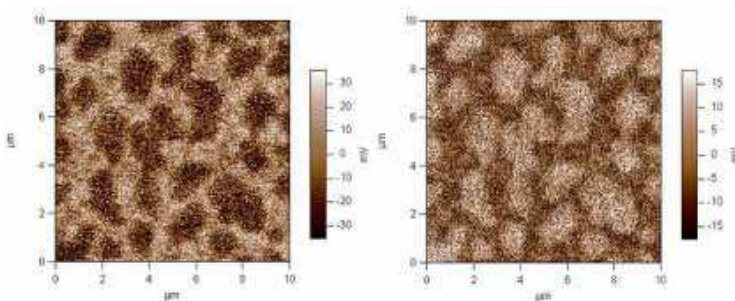
Fig. 13. In-phase image (input-i: left side) and quadrature image (input-q: right side) of sample B divided by phase image

According to Cleveland et al. (1998), if the amplitude of the cantilever is held constant, the sine of the phase angle of the driven vibration is then proportional to changes in the tip-sample energy dissipation. This means that images of the cantilever phase in tapping-mode AFM are closely related to maps of dissipation. Our phase images suggest that the bright area corresponds to a higher phase because a phase image is taken in repulsive mode. The bright area is more energy-dissipated than the dark area, which means the bright area is softer or more adhesive. Because the phase image was divided by the components of the in-phase (input-i) and the quadrature (input-q), the relation of the in-phase (input-i) and the quadrature (input-q) is converse. It seems that an in-phase image (input-i) has the same tendency as the force modulation image: its darker area corresponds to a softer area. In general, the relation between an in-phase image (input-i) and a quadrature image (input-q) is the relation between elasticity and viscosity. Our observations seem to experimentally support this relation. Figure 13 demonstrates that the bright area of the in-phase image has lower energy dissipation than the darker area, which means the bright area is harder or less adhesive. On the other hand, the darker area in figure 12 (the force modulation image) corresponds to a softer area. If ophthalmic lens surface is sticky, a lot of contaminants can easily attach to the lens surface. Fortunately, the lubricant material is fluorocarbon, which has low surface energy. Thus, the contaminant is easily removed from the lens surface wiping the surface with a cloth. From these results, in the case of sample B, it appears that these island structures are mixtures of soft regions and hard regions at the 10 μm scale.

Figure 14 illustrates the lubricant distribution of sample D by AFM topographic image and phase image at the 10 μm scale. Figure 15 shows the lubricant image of sample C by topographic image, phase image, in-phase image (input-i), and quadrature image (input-q) at the 1 μm scale. Figure 16 shows the lubricant image of sample C by topographic image, phase image, in-phase image (input-i), and quadrature image (input-q) at the 500 nm scale. The topographic image, phase image, in-phase (input-i), and quadrature image (input-q) of sample D at the 1 μm scale are shown in figure 17. Finally, the topographic image, phase image, in-phase (input-i), and quadrature image (input-q) of sample E at the 1 μm scale are shown in figure 18.

In the case of samples C, D, and E at the 10 μm scale, island structures cannot be observed by phase image, although it seems that the lubricant is homogeneous in these areas. However, samples C, D, and E reveal some island structures at smaller scales (i.e., 500 nm scale and 1 μm scale). We earlier discussed the relation between friction force image, force modulation image, and phase image. Nevertheless, the signal mark depends upon the measurement mode; these images reveal island structures in cases of similar morphology.

In the case of sample C, it seems that the grain is too small and some clusters gather with different dissipation energies. The topographic image of sample D reveals unevenness of grain, but the phase image clearly shows the grain boundary. This suggests that the grain boundary in sample D is accumulated lubricants rather than grain. On the other hand, sample E has grain but the grain boundary in the phase image is not clearly apparent. It seems that the lubricant in the grain boundary is in accord with the lubricant on the grain, and the lubricant of sample E is more homogenous than that of sample C or D.

In some ophthalmic lenses, island structures can be observed on the lens surface at the 10 μm scale, whereas in others it is necessary to use the 1 μm or 500 nm scale. From these lubricant images we have determined that the morphologies of the lubricants of commercial

ophthalmic lenses vary widely and thus perform differently in terms of wear property and dirt protection. Therefore, the methods described here are useful and suitable for investigation of lubricants on ophthalmic lens surfaces.
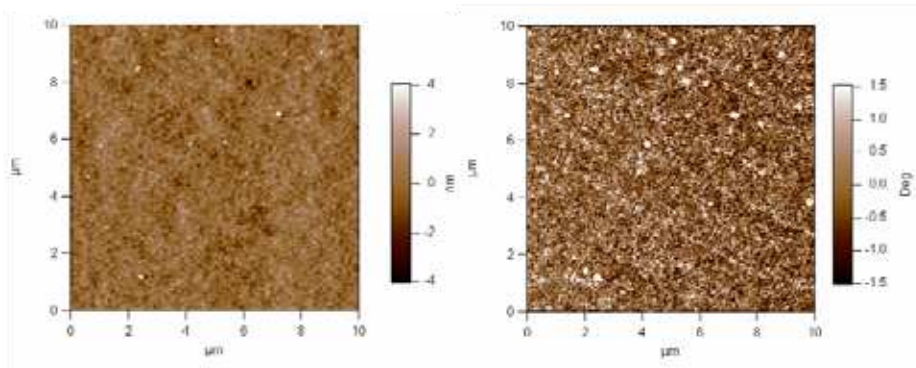

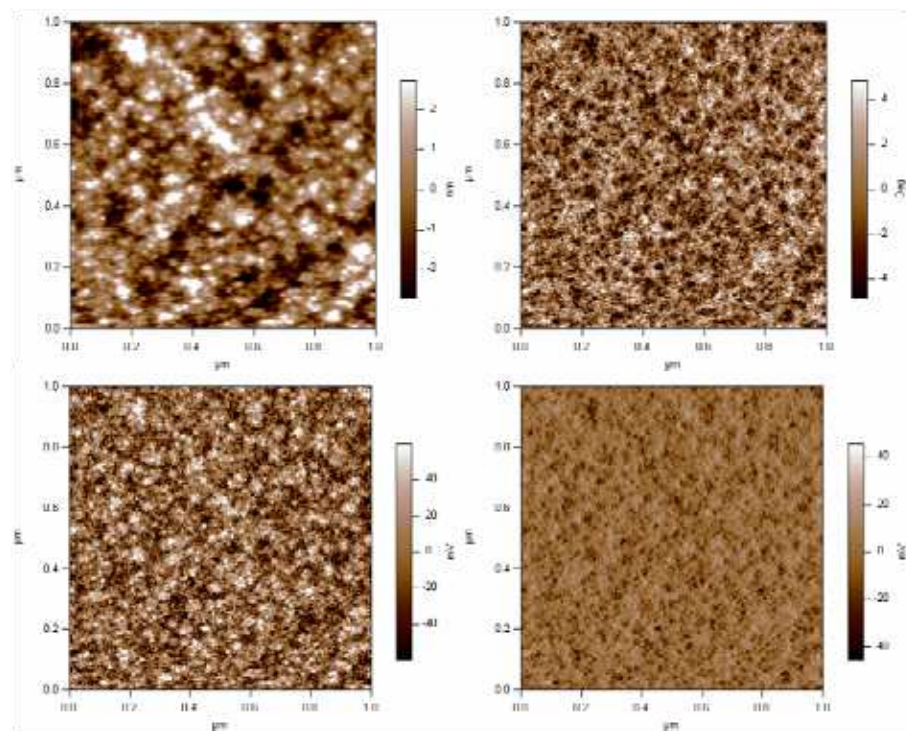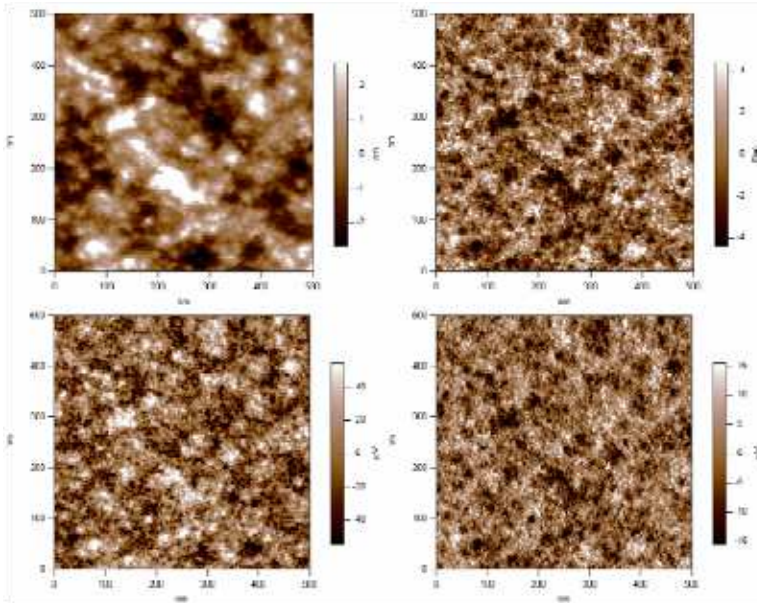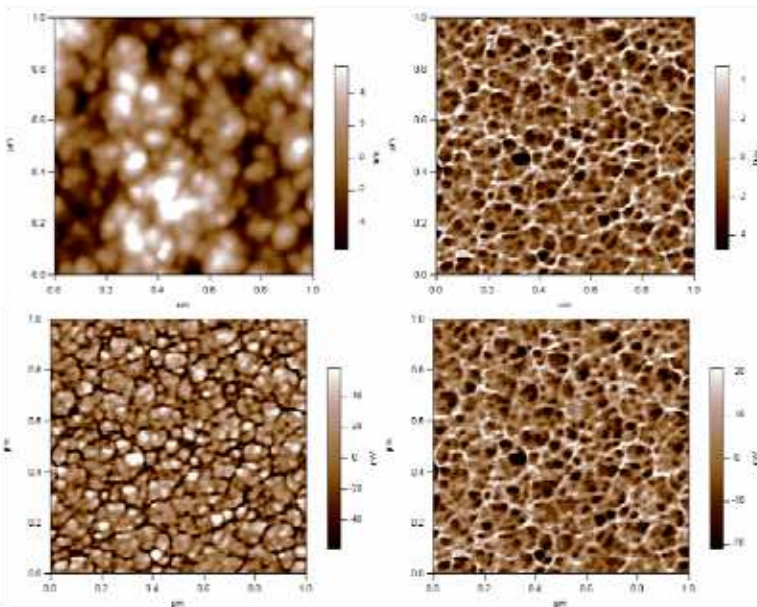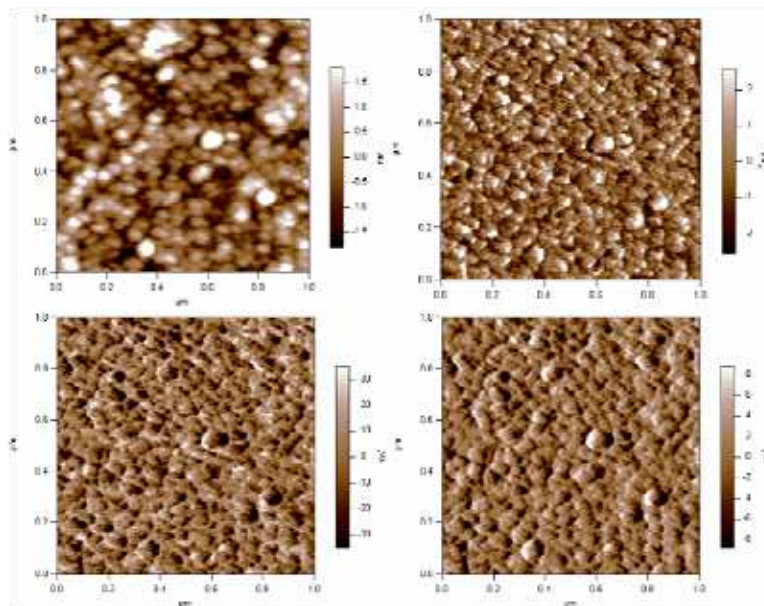Fig. 14. Topographic image (left side), phase image (right side) of sample D

Fig. 15. Topographic image (upper left), phase image (upper right), input-i image (lower left,) and input-q image (lower right) of sample C at the 1 μm scale

Fig. 16. Topographic image (upper left), phase image (upper right), input-i image (lower left), and input-q image (lower right) of sample C at the 500 nm scale

Fig. 17. Topographic image (upper left), phase image (upper right), input-i image (lower left), and input-q image (lower right) of sample D at the 1 μm scale

Fig. 18. Topographic image (upper left), phase image (upper right), input-i image (lower left), and input-q image (lower right) of sample E at the 1 μm scale

2.2.3 X-ray damage of lubricants and chimerical structures

Figure 19 shows the X-ray damage ratio of F_{1s} spectra for sample F, G, and H as a function of X-ray exposure time under the condition of X-ray power 300W and Mg-Kα source by XPS. Figures 20 - 22 show the changing chemical structure of C_{1s} for samples F-G as a function of exposure time (initial structure shown for reference, structure after 30 min, and structure after 60 min), as determined by XPS. Figure 23 shows the initial structure and of the mass spectra of positive fragment ions, as obtained by TOF-SIMS (upper spectrum: sample F, middle spectrum: sample G, lower spectrum: sample H). Figure 24 shows the mass spectra of positive fragment ions after 60 min X-ray exposure by XPS (upper spectrum: sample F, middle spectrum: sample G, lower spectrum: sample H). Figure 25 shows the mass spectra of negative fragment ions for sample F, as obtained by TOF-SIMS (upper spectrum: initial, lower spectrum: after 60 min, obtained by XPS). Table 3 summarized the film thickness and coverage ratio of lubricant before and after XPS damage.

From figure 19, we found that the X-ray damage in the case of sample F is greater than that in the case of sample G and sample H. In the case of sample G and sample H, the lubricant component of fluorine remained on the surface; fluorine was kept on approximately 80% on the surface after 60 min of exposure to X-rays. On the other hand, the lubricant component of sample F decreased by approximately 40% after exposure for 60 min.

On the basis of the initial structures shown in figure 23 and figure 25, it is concluded that the main structure of sample F has a side chain structure (-CF (CF$_3$)-CF$_2$-O-)m', similar to that in Fombline Y or Krytox. This periodic relation of 166 amu (C_3F_6O) continues up till mass numbers of approximately 5000 amu. In the case of magnetic disks, the high molecular structure of the lubricants was realized and maintained by dip coating or spin coating.
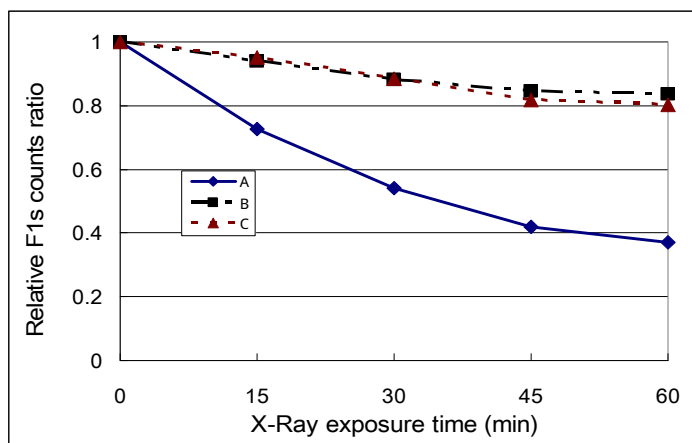
Fig. 19. Relationship between F1s intensity and X-Ray exposure time during XPS

However, the ophthalmic lens of lubricants was deposited by lamp heating methods into vacuum. Nevertheless, some main structure of lubricants was contained high-polymeric structures. On the other hand, the main structures of sample G and sample H has a straight chain structure without the side chain structures ($-CF_2-CF_2-O-$)m-(CF_2-O-)n, similar to the main structure of Fombline Z. From figure 20, 24 and 25, we found that the main chemical structure of lubricants for sample F is decreasing and destroying as a function of exposure time by XPS.
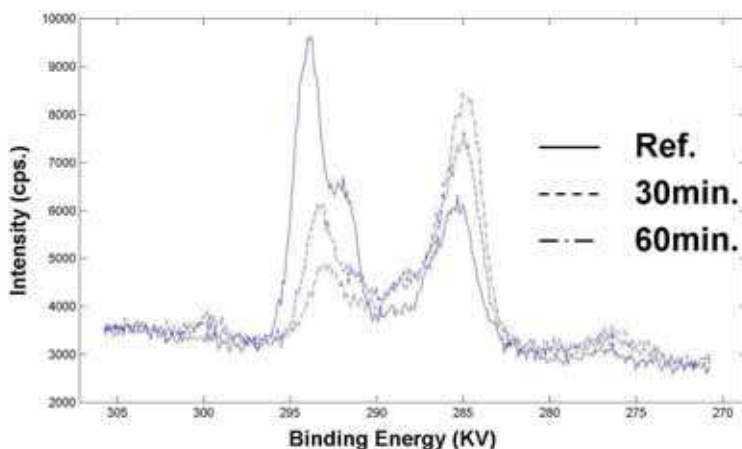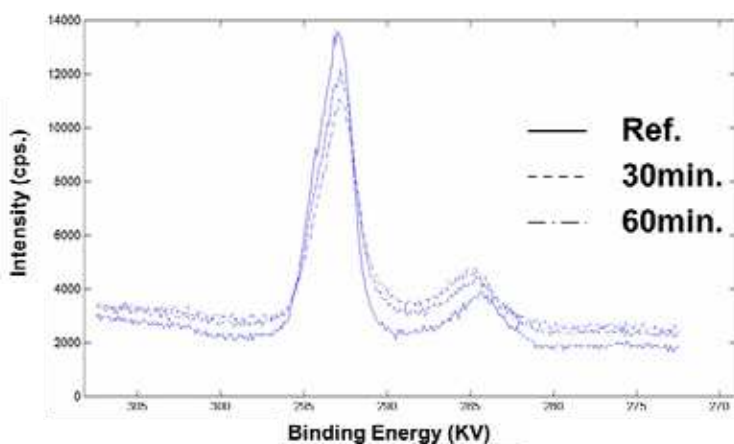

Fig. 20. Changing chemical structure of C_{1s} spectrum for sample F as a function of X-ray exposure time by XPS

These observations suggest that the straight chain structure of ($-CF_2-CF_2-O-$)m-(CF_2-O-)n is more robust to X-ray damage during XPS than the side chain structure ($-CF (CF_3)-CF_2-O-$)m'. We attribute this difference in the strength of the structures to the presence or absence of the chemical structure of the side chain. TEM or XPS measurement reveals that the film thickness

of the lubricants is 2–3 nm. According to Tani (1999), he found double steps on the lubricant film with 2.9 nm thickness that was almost completely cover the surface by the mean molecular radius of gyration with coil of lubricant molecular. Therefore, it seems that the 2-3 coils of lubricant molecular have been stacked on the surface of the ophthalmic lens.

In the case of sample F, the molecular interaction in the side chain structure of CF_3 is weaker than that in the straight chain structure of CF_2 because in CF_3, three-dimensional structures overlap and this leads to repulsion between fluorine atoms. Therefore, the damage due to exposure to X-rays during XPS in the case of sample F is more than that in the case of sample G or that in the case of sample H. It is predicted that the trend observed in the adhesion properties of lubricants will be the same as that observed in the case of these damages.

Fig. 21. Changing chemical structure of C_{1s} spectrum for sample G as a function of X-ray exposure time by XPS
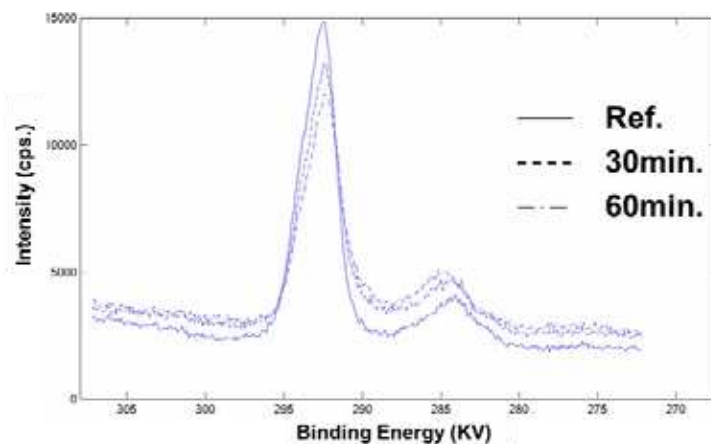
Fig. 22. Changing chemical structure of C_{1s} spectrum for sample H as a function of X-ray exposure time
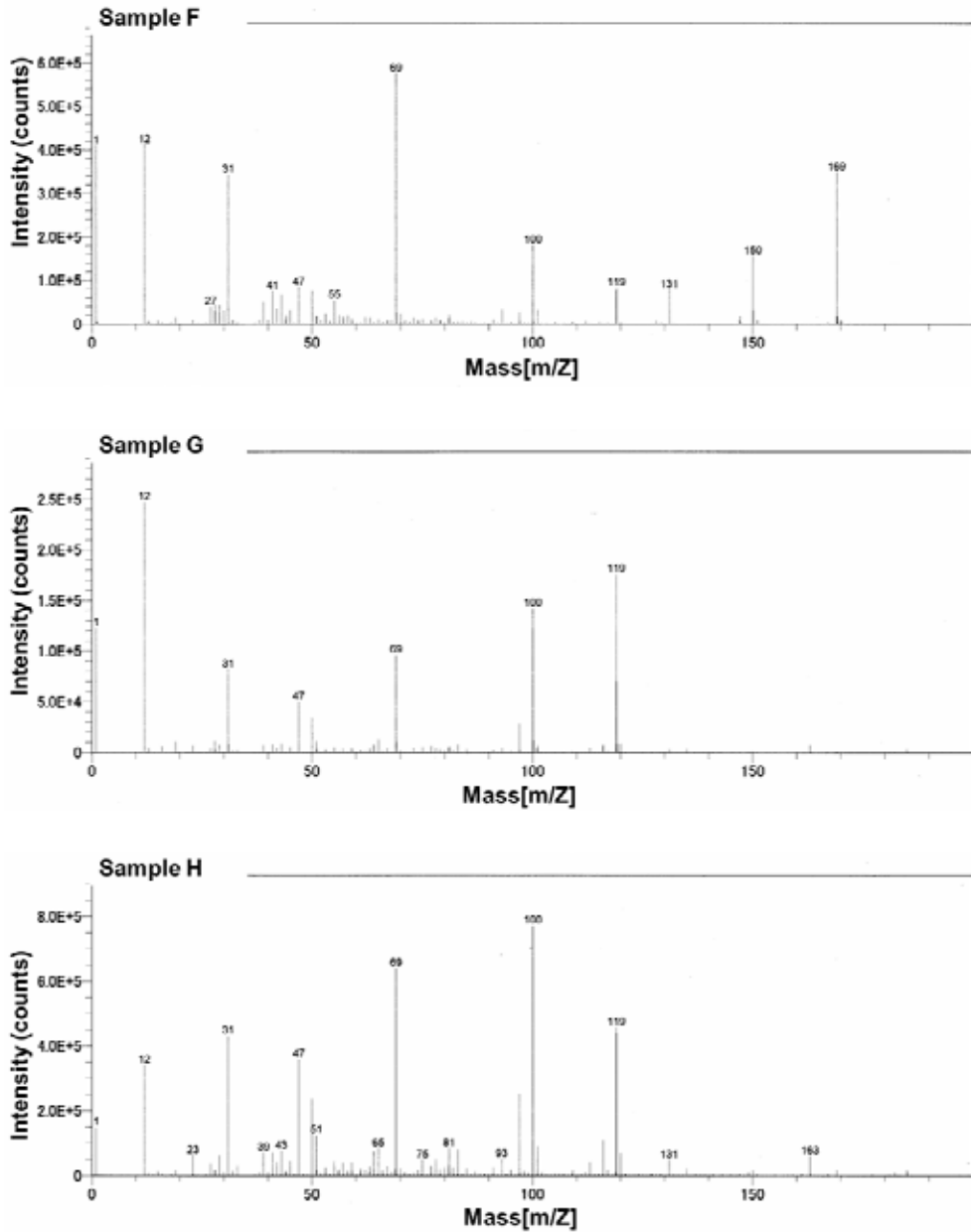
Fig. 23. Initial structure of the mass spectra of positive fragment ions, as determined by TOF-SIMS (upper spectrum: sample F, middle spectrum: sample G, lower spectrum: sample H)
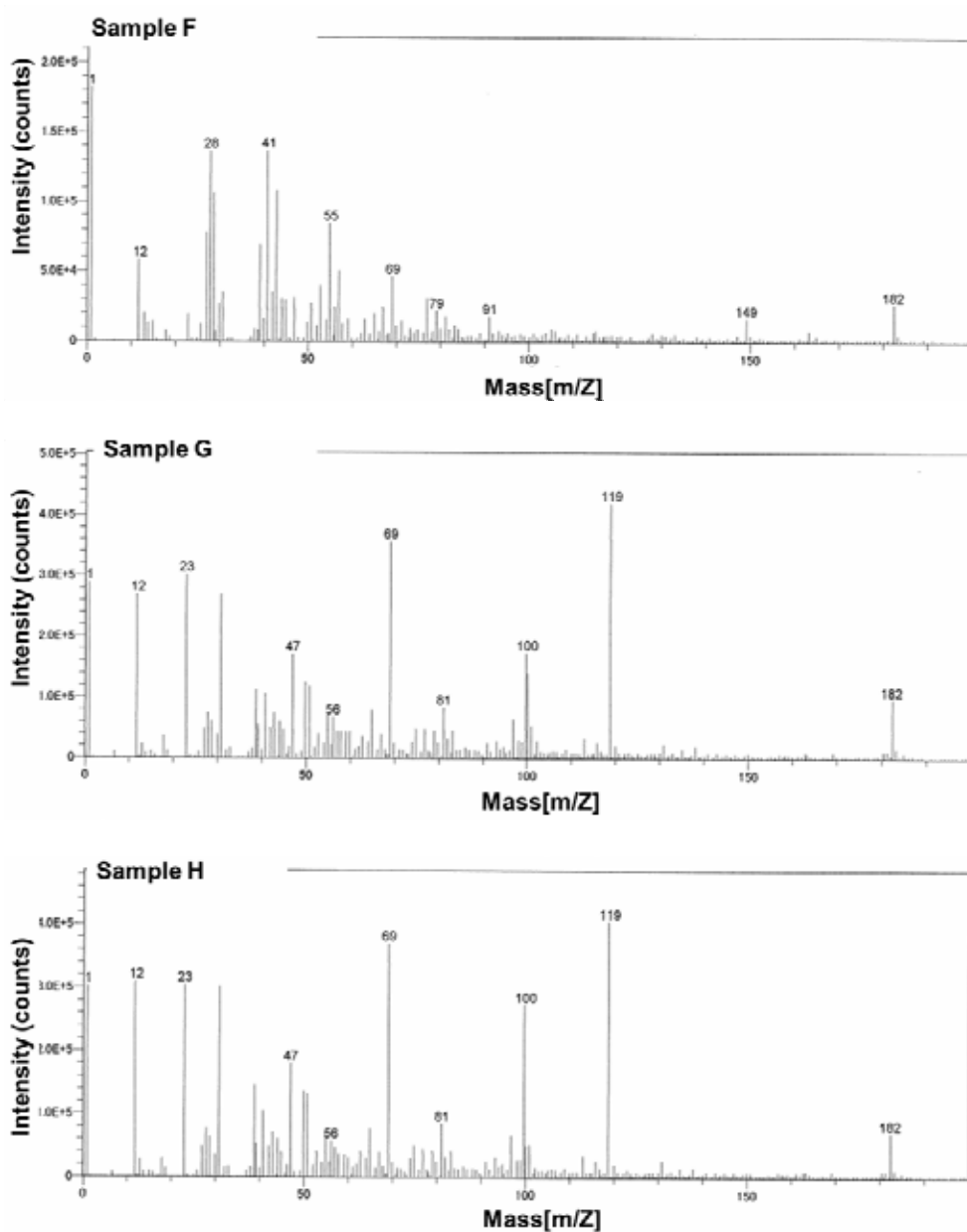
Fig. 24. The mass spectra of positive fragment ions after 60 min X-ray exposure by XPS, as determined by TOF-SIMS (upper spectrum: sample F, middle spectrum: sample G, lower spectrum: sample H)
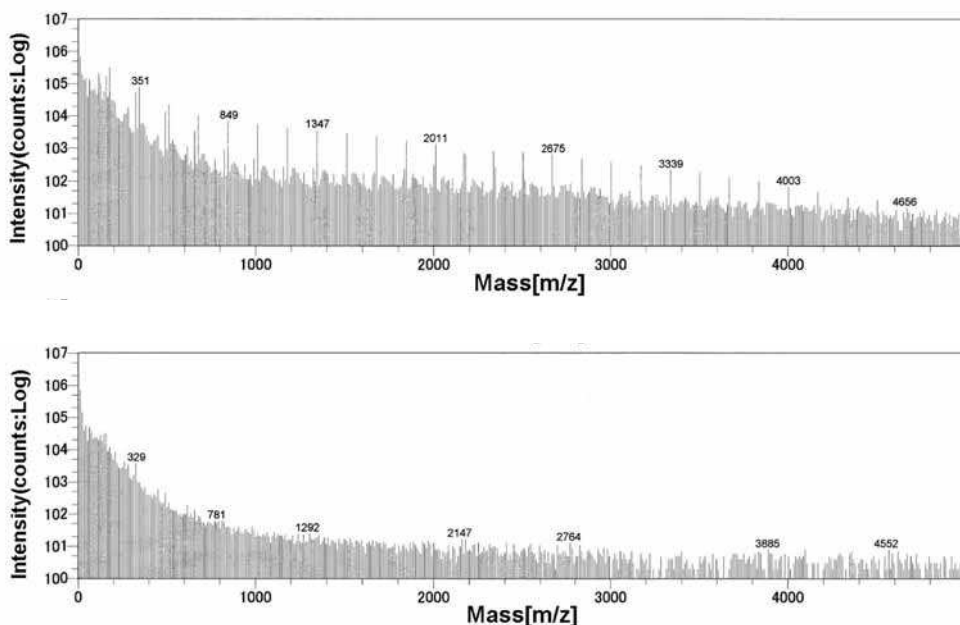
Fig. 25. Mass spectra of negative fragment ions for sample A, as determined by TOF-SIMS (upper spectrum: initial, lower spectrum: after 60 min X-ray exposure by XPS)

	Initial		After 60min X-ray explosured	
	Lub. film thickness (nm)	Lub. film coverage (%)	Lub. film thickness (nm)	Lub. film coverage (%)
Sample F	2.4-2.9	98 over	0.9-1.3	88-91
Sample G	2.3-2.7	98 over	1.8-2.2	94-95
Sample H	2.3-2.7	98 over	1.7-2.1	94-95

Table 3. Film thickness and coverage ratio of lubricant before and after XPS damage

2.2.4 Abrasion test

The water contact angle for sample F, sample G, and sample H before and after the abrasion test is listed in table 4. The XPS spectrum for each sample before and after abrasion test is shown in figures 26 – 28. Figures 29 – 31 show the topographic image and the phase image for each sample before and after abrasion test (image on the upper left image: initial topographic image, upper right image: initial phase image, lower left image: topographic image after abrasion test, lower right image: phase image after abrasion test).

The results in table 4 indicate that the water contact angles in the case of sample G and sample H decreased slightly after the abrasion test was performed. In contrast, the water contact angle of sample F decreased drastically from 116° to 89° after the sample was scratched by a 2 kg weight over 600 strokes. In the case of sample F, it seems that the water
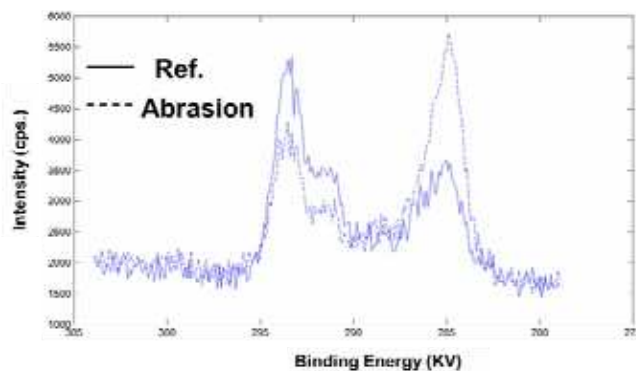
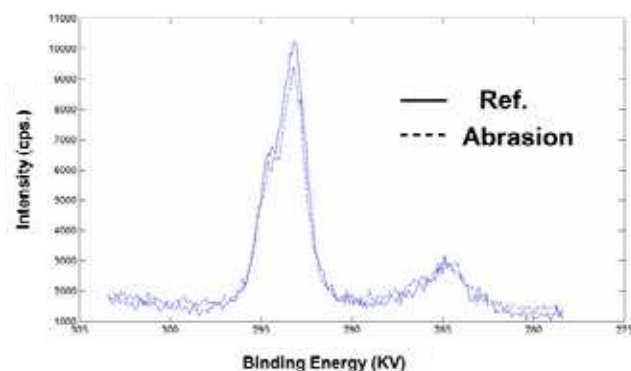Fig. 26. Changing chemical structure of C_{1s} spectrum for sample F before and after the abrasion test

Fig. 27. Changing chemical structure of C_{1s} spectrum for sample G before and after the abrasion test
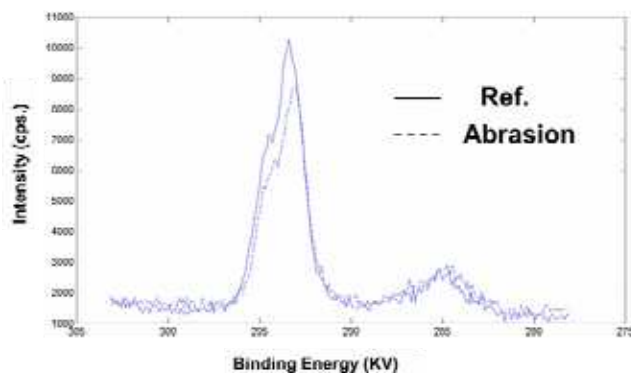

Fig. 28. Changing chemical structure of C_{1s} spectrum for sample H before and after the abrasion test
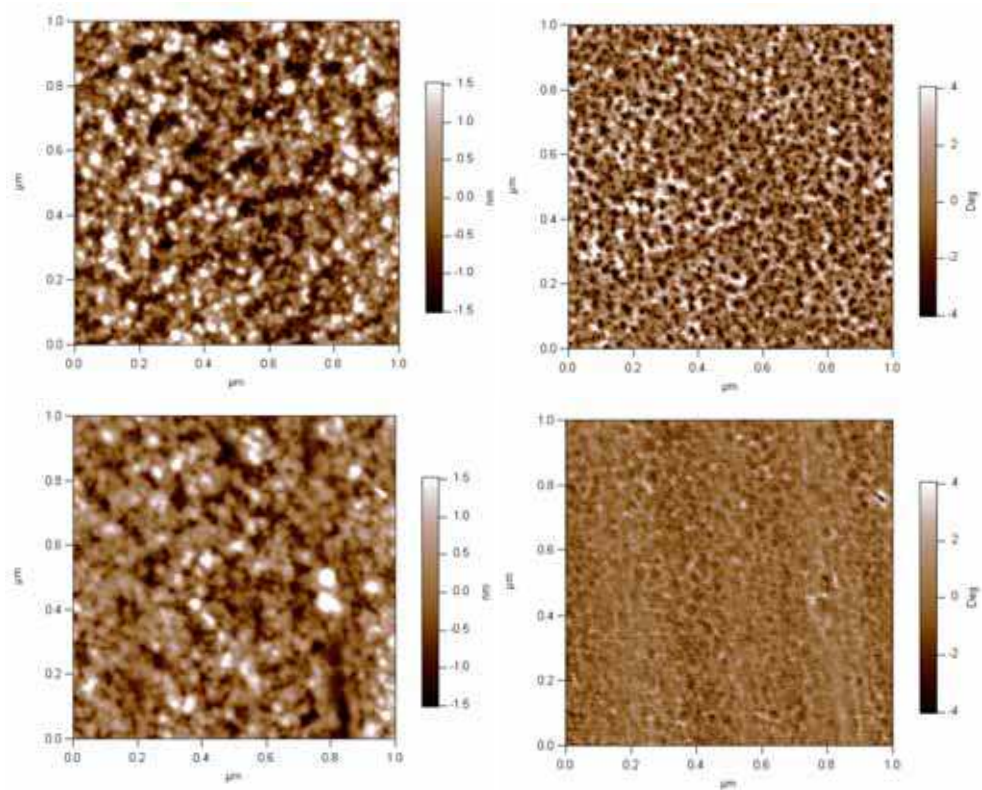
Fig. 29. Topographic image and phase image obtained for sample F (upper left image: initial topographic image, upper right image: initial phase image, lower left image: topographic image after abrasion test, lower right image: phase image after abrasion test)

repellant of lubricant was declined because it was decreased the lubricants quantity of sample F by abrasion test. A phase image that was obtained by AFM revealed the distribution of unevenness (roughness), the viscosity, elasticity, friction force, adhesion, and soft-hardness from the energy dissipation of interaction between tip and sample. In a previous study, we showed that the energy dissipation in the areas corresponding to bright areas in the phase image is greater than that in the areas corresponding to dark areas in the image. This result, along with a comparison of the phase image and force modulation image, reveals that the bright area is softer or more adhesive than the dark area. The initial phase images for each sample comprise a mixture of small soft areas and small hard areas (or small adhesive areas and small non-adhesive areas). In the case of sample F, a scratch is observed along the scan area in the image obtained after the abrasion test. Just like, the lubricants were removed by rubbing. Therefore, the water contact angle decreased when the lubricants were removed. On the other hand, in the case of sample G and sample H, we observed that the cluster of lubricants was larger than the initial cluster. Further, there is no scratch in the image obtained after the abrasion test. We guess that lubricants repeated the attaching and moving, the mixtures of soft regions and hard regions were grown by rubbing

process. Thus, there is no significant change in the water contact angle. These results indicate that the trend in lubricant damage during XPS agrees with the trend in durability during the abrasion test. Therefore, we found that we can select suitable lubricants for an ophthalmic lens by XPS measurement.
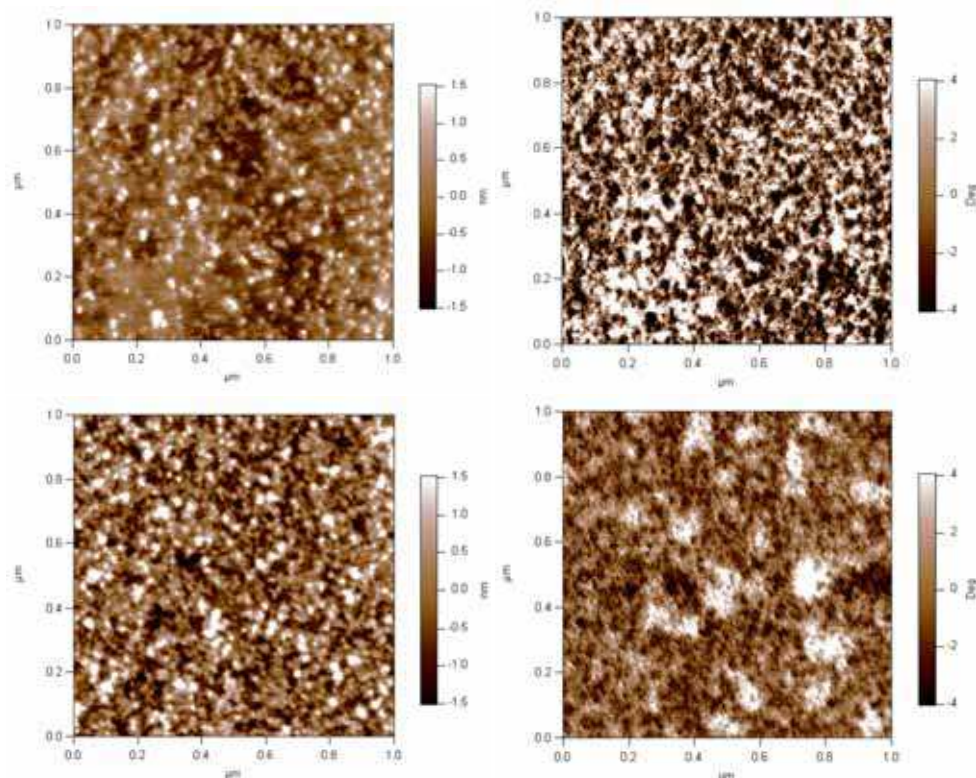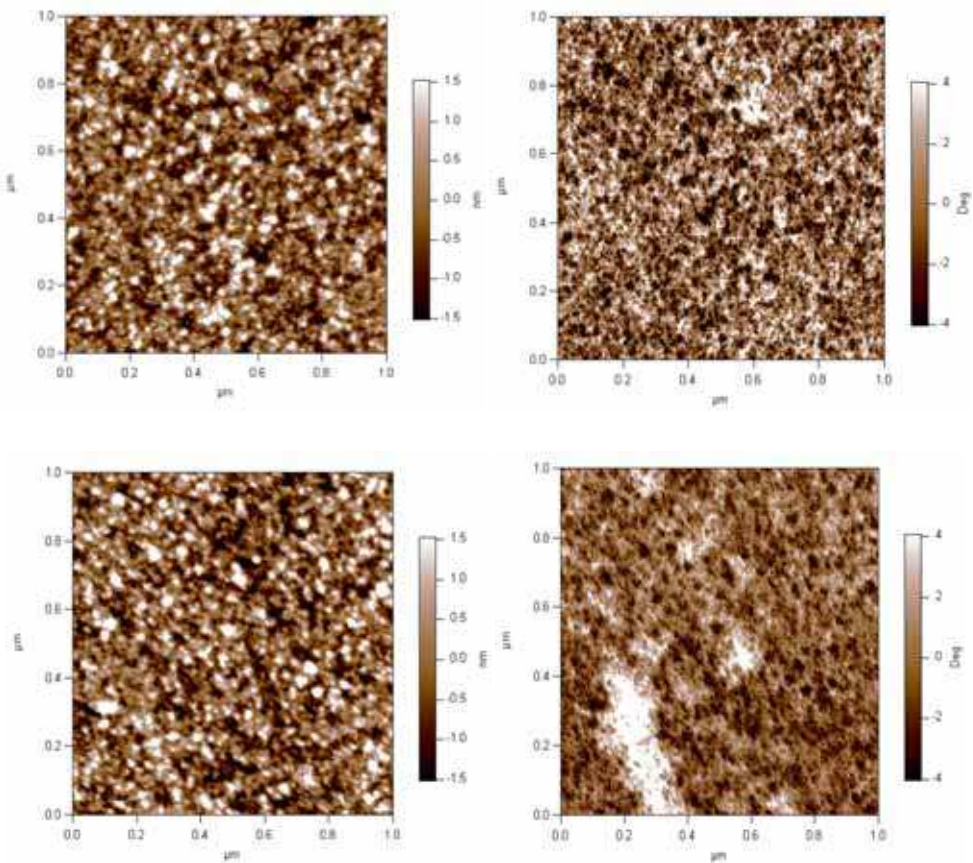

Fig. 30. Topographic image and phase image obtained for sample G (upper left image: initial topographic image, upper right image: initial phase image, lower left image: topographic image after abrasion test, lower right image: phase image after abrasion test)

	Initial		After abrasion test	
	Lub. film thickness (nm)	Contact angle	Lub. film thickness (nm)	Contact angle
Sample F	2.4-2.9	116°	1.1-1.5	89°
Sample G	2.3-2.7	110°	2.1-2.5	107°
Sample H	2.3-2.7	111°	1.9-2.5	108°

Table 4. Film thickness and water contact angle before and after the abrasion test

Fig. 31. Topographic image and phase image obtained for sample H (upper left image: initial topographic image, upper right image: initial phase image, lower left image: topographic image after abrasion test, lower right image: phase image after abrasion test)

3. Conclusion

We evaluated various methods for the analysis of lubricants on ophthalmic lenses. The lubricant film thickness can be directly determined by TEM measurement. The coverage ratio, the X-ray damage and the chemical structure can be investigated by XPS analysis. And also, TOF-SIMS analysis was used the investigation of X-ray damage and the chemical structure. In particular, AFM with an additional functional mode is a highly effective method for examining the morphology of lubricants; while determining the island structures of shapes with similar surface morphologies, it is more convenient to use phase images than friction force images and force modulation image. This information can be used to improve the tribological performance of ophthalmic lenses surface in order to meet customer demand.

4. Acknowledgment

5. References

Briggs, D. & Seah, M. P. (1990). Practical surface analysis 2'nd edition, John Wiley & Sons Ltd., pp209, ISBN 0471920819

Cleveland, J. P., Anczykowski, B., Schmid, A. E., & Elings, V. B. (1998). Applied Physics Letters, Vol. 72, No. 20, pp. 2613-2615, ISSN 0003-6951

Kimachi, Y., Yoshimura, F., Hoshino, M., & Terada, A. (1987), IEEE. Trans. mag., Vol.23, pp. 2392- 2394, ISSN 0018-9464

Matsuyama, K. (1997). J. of Japanese society of tribologists, Vol.42 pp. 823-828, ISSN 0915-1168

Mate, C. M., Lorenz, M. R. & Novotny, V. J. (1989). J. Chem. Phys., Vol.90, pp. 7550-7555, ISSN 0021-9606

Mate, C. M. & Novotny, V. J. (1991). J. Chem. Phys., Vol.94, pp. 8420-8427, ISSN 0021-9606

Newman, J. G. & Viswanathan, K. V. (1990). J. Vac. Sci. Technol. A8, pp. 2388-2392, ISSN 0734-2101

Novotny, V. J., Hussla, I., Turlet, J.-M., & Philopott, M. R. (1989). J. Chem. Phys., Vol. 90, pp. 5861-5868, ISSN 0021-9606

Novotny, V. J., Pan, X., & Bhatia, C. S. (1994). J. Vac. Sci. Technol. A12, pp. 2879-2886, ISSN 0734-2101

Sakane, Y. & Nakao, M. (1999). Magnetics Conference, INTERMAG 99, IEEE. Trans. mag., vol.35, pp. 2394-2396, ISBN 0-7803-5555-5

Seah, M. P. and Dench, W. A. (1979). Surface and interface analysis, Vol.1, pp. 2-11, ISSN 1096-9918

Tadokoro, N. & Osakabe, K. (2001). Proc. Int. Tribol. Conference Nagasaaki 2000, pp. 2191-2196, ISBN 4-9900139-6-4

Tadokoro, N., Yuki M., & Osakabe, K. (2003). Applied surface science, 203-204, pp. 72-77, ISSN 0169-4332

Tadokoro, N., Khraikratoke, S., Jamnongpian, P., Maeda, A., Komine, Y., Pavarinpong, N., Suyjantuk, S., & Iwata, N. (2009). Proc. World. Tribol. Congress 2009, pp. 749, ISBN 978-4-9900139-9-8

Tadokoro, N., Pannakarn, S., Khraikratoke S., Kamura, H., & Iwata, N. (2010). Proc. the 8th ICCG8, pp. 343-348, ISBN 978-3-00-031387-5

Tadokoro, N., Pannakarn, S., Wisuthtatip, J., Kunchoo, S., Parnich, V., Takashiba, K., Shimizu, K., and Higuchi, H. (2011). J. of Surface analysis, Vol.13 pp. 190-193, ISSN 1341-1756

Tani, H. (1999). Magnetics Conference, INTERMAG 99, IEEE. Trans. mag., vol.35, pp.2397-2399, ISBN 0-7803-5555-5

Toney, M. F., Mate C. M., & Pocker, D. (1991). IEEE. Trans. mag., Vol.34, pp. 1774-1776, ISSN 0018-9464
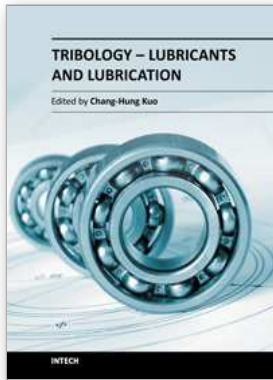
Tribology - Lubricants and Lubrication

Edited by Dr. Chang-Hung Kuo

In the past decades, significant advances in tribology have been made as engineers strive to develop more reliable and high performance products. The advancements are mainly driven by the evolution of computational techniques and experimental characterization that leads to a thorough understanding of tribological process on both macro- and microscales. The purpose of this book is to present recent progress of researchers on the hydrodynamic lubrication analysis and the lubrication tests for biodegradable lubricants.

How to reference

In order to correctly reference this scholarly work, feel free to copy and paste the following:

Nobuyuki Tadokoro (2011). Characterization of Lubricant on Ophthalmic Lenses, Tribology - Lubricants and Lubrication, Dr. Chang-Hung Kuo (Ed.), ISBN: 978-953-307-371-2, InTech, Available from: http://www.intechopen.com/books/tribology-lubricants-and-lubrication/characterization-of-lubricant-on-ophthalmic-lenses